

Analysis and Improvement of the Consistency of Extended Kalman Filter based SLAM

Guoquan P. Huang, Anastasios I. Mourikis and Stergios I. Roumeliotis
Dept. of Computer Science and Engineering, University of Minnesota, Minneapolis, MN 55455
email: {ghuang|mourikis|stergios}@cs.umn.edu

Abstract—In this work, we study the inconsistency of EKF-based SLAM from the perspective of observability. We analytically prove that when the Jacobians of the state and measurement models are evaluated at the latest state estimates during every time step, the linearized error-state system model of the EKF-based SLAM has observable subspace of dimension higher than that of the actual, nonlinear, SLAM system. As a result, the covariance estimates of the EKF undergo reduction in directions of the state space where no information is available, which is a primary cause of inconsistency. To address this issue, a new “First Estimates Jacobian” (FEJ) EKF is proposed, which is shown to perform better in terms of consistency. In the FEJ-EKF, the filter Jacobians are calculated using the first-ever available estimates for each state variable, which insures that the observable subspace of the error-state system model is of the same dimension as that of the underlying nonlinear SLAM system. The theoretical analysis is validated through extensive simulations.

I. INTRODUCTION

For autonomous vehicles exploring unknown environments, the ability to perform simultaneous localization and mapping (SLAM) is essential. Among the numerous algorithms developed thus far for the SLAM problem, the extended Kalman filter (EKF) remains one of the most popular ones, and has been used in several practical applications. In this work, we address the *consistency* issue of the EKF-SLAM algorithm, which has recently received considerable attention [1]–[5]. As defined in [6], a state estimator is consistent if the estimation errors (i) are zero-mean, and (ii) have covariance matrix smaller or equal to the one calculated by the filter. Consistency is one of the primary criteria for evaluating the performance of any estimator; if an estimator is inconsistent, then the accuracy of the produced state estimates is unknown, which in turn makes the estimator unreliable.

Since SLAM is a nonlinear estimation problem, no provably consistent estimator can be constructed for it. The consistency of every estimator has to be evaluated experimentally. In particular for the *standard* EKF-SLAM algorithm, there exists significant empirical evidence showing that the computed state estimates tend to be *inconsistent*. The first work to draw attention to this issue was that of Julier and Uhlmann [3]. Specifically, in [3] it was observed that when a stationary robot measures the relative position of a new landmark multiple times, the estimated variance of the robot’s orientation becomes smaller. Since the observation of a previously unseen feature does not provide any information about the robot’s state, this reduction is “artificial,” and leads to inconsistency. Bailey *et al.* [2] examined several symptoms of the inconsistency of the standard EKF algorithm, and argued, based on

simulation results, that the uncertainty in the robot orientation is the main cause of the inconsistency of EKF-SLAM. The work of [5] further confirmed the empirical findings in [2], and argued by example that in EKF-SLAM the inconsistency is always in the form of overconfident estimates (i.e., computed covariances smaller than the actual ones).

The aforementioned works have described several symptoms of inconsistency that appear in the standard EKF-SLAM. However, they have not conducted a detailed analysis into the exact cause of the inconsistency (with the exception of [3] for the special case of a stationary robot). In this paper, we investigate in depth one of the fundamental causes of inconsistency. In particular, we revisit this problem from a new perspective, i.e., by analyzing the observability properties of the filter’s error-state system model. The main contributions of this work are the following:

- Through an observability analysis, we prove that the standard EKF-SLAM employs an error-state system model that has an unobservable subspace of dimension two, even though the underlying nonlinear system model has three unobservable degrees of freedom (corresponding to the position and orientation of the global reference frame). This is a primary cause of filter inconsistency.
- We propose a new algorithm, termed *First Estimates Jacobian* (FEJ)-EKF, which improves the estimator’s consistency during SLAM. Specifically, we show analytically that when the EKF Jacobians are computed using the first-ever available estimates for each of the state variables, the error-state model has the *same* observability properties as the underlying nonlinear model. As a result of these properties, the new FEJ-EKF outperforms, in terms of accuracy and consistency, alternative approaches to this problem [1].

II. SLAM OBSERVABILITY ANALYSIS

The observability properties of SLAM have been studied in few only cases in the literature. In particular, [7], [8] investigated the observability of a simple *linear time invariant* (LTI) SLAM system, and showed that it is unobservable. On the other hand, in [9] the observability of the nonlinear SLAM system was studied, using the nonlinear observability rank condition developed by Hermann and Krener [10]. This work proved that the underlying, nonlinear, SLAM system is unobservable, with three unobservable degrees of freedom. However, to the best of our knowledge, an analysis of the observability properties of the EKF’s linearized error-state system model does not exist to date. As shown in this paper,

these properties play a significant role in determining the consistency of the filter.

In the following, after presenting the equations of the standard EKF-SLAM formulation, we compare its observability properties with those of the underlying nonlinear system, and use this analysis to draw conclusions about the consistency of the filter. To preserve the clarity of the presentation, in this section we consider the case where a *single* landmark is included in the state vector. However, the conclusions drawn in this case can be readily extended to the general case of multiple landmarks. We note that, due to space limitations, some intermediate steps of the derivations have been omitted; the interested reader is referred to [11] for details.

A. Standard EKF-SLAM

In the standard formulation of SLAM, the state vector comprises the robot pose and the landmarks' positions in the global frame. Thus, at time-step k the state vector is given by

$$\mathbf{x}_k = [\mathbf{p}_{R_k}^T \quad \phi_{R_k} \quad \mathbf{p}_L^T]^T = [\mathbf{x}_{R_k}^T \quad \mathbf{p}_L^T]^T \quad (1)$$

where $\mathbf{x}_{R_k} = [\mathbf{p}_{R_k}^T \quad \phi_{R_k}]^T$ denotes the robot pose (position and orientation), and \mathbf{p}_L is the landmark position.

1) *EKF Propagation*: In the propagation step, the robot's odometry measurements are processed to obtain an estimate of the pose change between two consecutive time steps, and then employed in the EKF to propagate the robot state estimate. On the other hand, since the landmark is static, its estimate does not change with the incorporation of a new odometry measurement. The EKF propagation equations are given by:¹

$$\hat{\mathbf{p}}_{R_{k+1}|k} = \hat{\mathbf{p}}_{R_k|k} + \mathbf{C}(\hat{\phi}_{R_k|k})^{R_k} \hat{\mathbf{p}}_{R_{k+1}} \quad (2)$$

$$\hat{\phi}_{R_{k+1}|k} = \hat{\phi}_{R_k|k} + {}^{R_k} \hat{\phi}_{R_{k+1}} \quad (3)$$

$$\hat{\mathbf{p}}_{L_{k+1}|k} = \hat{\mathbf{p}}_{L_k|k} \quad (4)$$

where $\mathbf{C}(\cdot)$ denotes the 2×2 rotation matrix, and ${}^{R_k} \hat{\mathbf{x}}_{R_{k+1}} = [{}^{R_k} \hat{\mathbf{p}}_{R_{k+1}}^T \quad {}^{R_k} \hat{\phi}_{R_{k+1}}]^T$ is the odometry-based estimate of the robot's motion between time-steps k and $k+1$. This estimate is corrupted by zero-mean, white Gaussian noise $\mathbf{w}_k = {}^{R_k} \mathbf{x}_{R_{k+1}} - {}^{R_k} \hat{\mathbf{x}}_{R_{k+1}}$, with covariance matrix \mathbf{Q}_k .

In addition to the state propagation equations, the linearized error-state propagation equation is necessary for the EKF. This is given by:

$$\begin{aligned} \tilde{\mathbf{x}}_{k+1|k} &= \begin{bmatrix} \Phi_{R_k} & \mathbf{0}_{3 \times 2} \\ \mathbf{0}_{2 \times 3} & \mathbf{I}_2 \end{bmatrix} \begin{bmatrix} \tilde{\mathbf{x}}_{R_k|k} \\ \tilde{\mathbf{x}}_{L_k|k} \end{bmatrix} + \begin{bmatrix} \mathbf{G}_{R_k} \\ \mathbf{0}_{2 \times 2} \end{bmatrix} \mathbf{w}_k \\ &\triangleq \Phi_k \tilde{\mathbf{x}}_{k|k} + \mathbf{G}_k \mathbf{w}_k \end{aligned} \quad (5)$$

where Φ_{R_k} and \mathbf{G}_{R_k} are obtained from the state propagation equations (2)-(3) as [11]:

$$\Phi_{R_k} = \begin{bmatrix} \mathbf{I}_2 & \mathbf{J}\mathbf{C}(\hat{\phi}_{R_k|k})^{R_k} \hat{\mathbf{p}}_{R_{k+1}} \\ \mathbf{0}_{1 \times 2} & 1 \end{bmatrix} \quad (6)$$

¹Throughout this paper the subscript $\ell|j$ refers to the estimate of a quantity at time-step ℓ , after all measurements up to time-step j have been processed. \hat{x} is used to denote the estimate of a random variable x , while $\tilde{x} = x - \hat{x}$ is the error in this estimate. $\mathbf{0}_{m \times n}$ and $\mathbf{1}_{m \times n}$ denote $m \times n$ matrices of zeros and ones, respectively, while \mathbf{I}_n is the $n \times n$ identity matrix. Finally, we use the concatenated forms $s\phi$ and $c\phi$ to denote the $\sin \phi$ and $\cos \phi$ functions, respectively.

$$\equiv \begin{bmatrix} \mathbf{I}_2 & \mathbf{J}(\hat{\mathbf{p}}_{R_{k+1}|k} - \hat{\mathbf{p}}_{R_k|k}) \\ \mathbf{0}_{1 \times 2} & 1 \end{bmatrix} \quad (7)$$

$$\mathbf{G}_{R_k} = \begin{bmatrix} \mathbf{C}(\hat{\phi}_{R_k|k}) & \mathbf{0}_{2 \times 1} \\ \mathbf{0}_{1 \times 2} & 1 \end{bmatrix} \quad (8)$$

$$\text{where } \mathbf{J} \triangleq \begin{bmatrix} 0 & -1 \\ 1 & 0 \end{bmatrix}.$$

It is important to point out that the form of the propagation equations presented above is general, and holds for any robot kinematic model (e.g., unicycle, bicycle, or Ackerman model). For example, if the unicycle model is used, and we employ the approximation that the velocity and heading are constant during each propagation interval, we obtain ${}^{R_k} \hat{\mathbf{x}}_{R_{k+1}} = [v_{m_k} \delta t \quad 0 \quad \omega_{m_k} \delta t]^T$, where v_{m_k} and ω_{m_k} are the linear and rotational velocity measurements, respectively, and δt is the sampling period. Substitution in (2)-(3) yields the familiar robot pose propagation equations:

$$\hat{\mathbf{p}}_{R_{k+1}|k} = \hat{\mathbf{p}}_{R_k|k} + \begin{bmatrix} v_{m_k} \delta t c(\hat{\phi}_{R_k|k}) \\ v_{m_k} \delta t s(\hat{\phi}_{R_k|k}) \end{bmatrix} \quad (9)$$

$$\hat{\phi}_{R_{k+1}|k} = \hat{\phi}_{R_k|k} + \omega_{m_k} \delta t \quad (10)$$

Similarly, the commonly used expressions for the matrices Φ_{R_k} and \mathbf{G}_{R_k} can be derived from (5), (6) and (8) (cf. [11]).

2) *EKF Update*: The measurement used for updates in the EKF is a function of the relative position of the landmark with respect to the robot:

$$\mathbf{z}_k = \mathbf{h}(\mathbf{x}_k) + \mathbf{v}_k = \mathbf{h}(\mathbf{C}^T(\phi_{R_k})(\mathbf{p}_{L_k} - \mathbf{p}_{R_k})) + \mathbf{v}_k \quad (11)$$

where \mathbf{v}_k is zero-mean Gaussian measurement noise with covariance \mathbf{R}_k . In this work, we allow \mathbf{h} to be *any* 2-dimensional measurement function, as long as it is invertible (i.e., as long as we can fully determine an estimate of the robot-relative landmark position from \mathbf{z}_k). For instance, this is the case when \mathbf{z}_k is a direct measurement of relative position, a pair of range and bearing measurements, two bearing measurements from the cameras of a stereo pair, etc. Generally, the measurement function is nonlinear, and hence it is linearized for use in the EKF. The linearized measurement-error equation is given by

$$\begin{aligned} \tilde{\mathbf{z}}_k &\simeq [\mathbf{H}_{R_k} \quad \mathbf{H}_{L_k}] \begin{bmatrix} \tilde{\mathbf{x}}_{R_k|k-1} \\ \tilde{\mathbf{x}}_{L_k|k-1} \end{bmatrix} + \mathbf{v}_k \\ &\triangleq \mathbf{H}_k \tilde{\mathbf{x}}_{k|k-1} + \mathbf{v}_k \end{aligned} \quad (12)$$

where \mathbf{H}_{R_k} and \mathbf{H}_{L_k} are the Jacobians of \mathbf{h} with respect to the robot pose and the landmark position, respectively, evaluated at the state estimate $\hat{\mathbf{x}}_{k|k-1}$. Using the chain rule of differentiation, these are computed as:

$$\mathbf{H}_{R_k} = (\nabla \mathbf{h}_k) \mathbf{C}^T(\hat{\phi}_{R_k|k-1}) [-\mathbf{I}_2 \quad -\mathbf{J}(\hat{\mathbf{p}}_{L_k|k-1} - \hat{\mathbf{p}}_{R_k|k-1})] \quad (13)$$

$$\mathbf{H}_{L_k} = (\nabla \mathbf{h}_k) \mathbf{C}^T(\hat{\phi}_{R_k|k-1}) \quad (14)$$

where $\nabla \mathbf{h}_k$ denotes the Jacobian of \mathbf{h} with respect to the robot-relative landmark position (i.e., with respect to the vector ${}^{R_k} \mathbf{p}_L = \mathbf{C}^T(\phi_{R_k})(\mathbf{p}_L - \mathbf{p}_{R_k})$), evaluated at the state estimate $\hat{\mathbf{x}}_{k|k-1}$.

B. Nonlinear Observability Analysis for SLAM

Before studying the observability properties of the EKF system model, we conduct the observability analysis for the underlying continuous-time nonlinear SLAM system. By comparing the properties of the actual, nonlinear, system with those of the EKF system model, we will be able to identify a fundamental shortcoming of the standard EKF formulation, which leads to filter inconsistency. The nonlinear observability analysis is based on the *observability rank condition* introduced in [10]. Specifically, Theorem 3.11 in [10] proves that “if a nonlinear system is locally weakly observable, the observability rank condition is satisfied generically”. We here show that the SLAM system does not satisfy the observability rank condition, and thus it is not locally weakly observable nor locally observable.

For the continuous-time analysis we employ a unicycle kinematic model, and a relative-position measurement model, although identical conclusions can be reached if different models are used [9]. The system model in continuous-time form is given by

$$\begin{aligned} \begin{bmatrix} \dot{x}_R(t) \\ \dot{y}_R(t) \\ \dot{\phi}_R(t) \\ \dot{x}_L(t) \\ \dot{y}_L(t) \end{bmatrix} &= \begin{bmatrix} c\phi(t) \\ s\phi(t) \\ 0 \\ 0 \\ 0 \end{bmatrix} v(t) + \begin{bmatrix} 0 \\ 0 \\ 1 \\ 0 \\ 0 \end{bmatrix} \omega(t) \\ \Rightarrow \dot{\mathbf{x}}(t) &= \mathbf{f}_1 v(t) + \mathbf{f}_2 \omega(t) \end{aligned} \quad (15)$$

where $\mathbf{u} \triangleq [v \ \omega]^T$ is the control input, consisting of linear and rotational velocity. The continuous-time relative-position measurement model is described by the expressions:

$$\begin{aligned} \mathbf{z}(t) &= \mathbf{C}^T(\phi(t))(\mathbf{p}_L - \mathbf{p}_R(t)) \\ &= \begin{bmatrix} c\phi(t)(x_L(t) - x_R(t)) + s\phi(t)(y_L(t) - y_R(t)) \\ -s\phi(t)(x_L(t) - x_R(t)) + c\phi(t)(y_L(t) - y_R(t)) \end{bmatrix} \\ &= \begin{bmatrix} h_1(\mathbf{x}) \\ h_2(\mathbf{x}) \end{bmatrix} \end{aligned} \quad (16)$$

The observability analysis for the system model described in (15) and (16) proceeds by first computing the space spanned by all the k th order Lie derivatives $L_{\mathbf{f}_j}^k h_i$ (for $k \in \mathbb{N}$, $j = 1, 2$, $i = 1, 2$), which we denote by \mathcal{G} . The space $d\mathcal{G}$, spanned by the gradients of the elements of \mathcal{G} is [11]:

$$\begin{aligned} d\mathcal{G} &= \text{span} \\ &\left[\begin{array}{cccc} s\phi & -c\phi & -c\phi(x_L - x_R) - s\phi(y_L - y_R) & -s\phi & c\phi \\ c\phi & s\phi & s\phi(x_L - x_R) - c\phi(y_L - y_R) & -c\phi & -s\phi \end{array} \right] \end{aligned} \quad (17)$$

The matrix shown above is the “observability matrix” for the nonlinear SLAM system under consideration. Clearly, the rank of this matrix is two, and thus the system is unobservable. Intuitively, this is a consequence of the fact that we cannot gain *absolute*, but rather only *relative* state information from the available measurements.

Even though the notion of an “unobservable subspace” cannot be strictly defined for this system, by examining the physical interpretation of the basis of $d\mathcal{G}^\perp$, which is the subspace orthogonal to $d\mathcal{G}$, we will gain useful information

for our analysis in Section II-C. By inspection, we see that one possible basis for the space $d\mathcal{G}^\perp$ is given by

$$d\mathcal{G}^\perp = \text{span} \begin{bmatrix} 1 & 0 & -y_R \\ 0 & 1 & x_R \\ 0 & 0 & 1 \\ 1 & 0 & -y_L \\ 0 & 1 & x_L \end{bmatrix} = \text{span} [\mathbf{n}_1 \ \mathbf{n}_2 \ \mathbf{n}_3] \quad (18)$$

From the structure of the vectors \mathbf{n}_1 and \mathbf{n}_2 we see that a change in the state by $\Delta\mathbf{x} = \alpha\mathbf{n}_1 + \beta\mathbf{n}_2$, $\alpha, \beta \in \mathbb{R}$ corresponds to a “shifting” of the $x - y$ plane by α units along x , and by β units along y . Thus, if the robot and landmark positions are shifted equally, the states \mathbf{x} and $\mathbf{x} + \Delta\mathbf{x}$ will be indistinguishable given the measurements. To better understand the physical meaning of \mathbf{n}_3 , we consider the case where the $x - y$ plane is rotated by a small angle $\delta\phi$. Rotating the coordinate system transforms any point $\mathbf{x} = [x \ y]^T$ to a point $\mathbf{x}' = [x' \ y']^T$, given by:

$$\begin{bmatrix} x' \\ y' \end{bmatrix} = \mathbf{C}(\delta\phi) \begin{bmatrix} x \\ y \end{bmatrix} \simeq \begin{bmatrix} 1 & -\delta\phi \\ \delta\phi & 1 \end{bmatrix} \begin{bmatrix} x \\ y \end{bmatrix} = \begin{bmatrix} x \\ y \end{bmatrix} + \delta\phi \begin{bmatrix} -y \\ x \end{bmatrix}$$

where we have employed the small-angle approximations $c(\delta\phi) \simeq 1$ and $s(\delta\phi) \simeq \delta\phi$. Using this result, we see that if the plane containing the robot and landmarks is rotated by $\delta\phi$, the SLAM state vector will change to

$$\mathbf{x}' = \begin{bmatrix} x'_R \\ y'_R \\ \phi'_R \\ x'_L \\ y'_L \end{bmatrix} \simeq \begin{bmatrix} x_R \\ y_R \\ \phi_R \\ x_L \\ y_L \end{bmatrix} + \delta\phi \begin{bmatrix} -y_R \\ x_R \\ 1 \\ -y_L \\ x_L \end{bmatrix} = \mathbf{x} + \delta\phi\mathbf{n}_3 \quad (19)$$

which indicates that the vector \mathbf{n}_3 corresponds to a rotation of the $x - y$ plane. Since $\mathbf{n}_3 \in d\mathcal{G}^\perp$, this result shows that any such rotation is unobservable, and will cause no change to the measurements. The preceding analysis for the meaning of the basis vectors of $d\mathcal{G}^\perp$ agrees with intuition, which dictates that the *global coordinates* of the state vector in SLAM (rotation and translation) are unobservable.

C. EKF-SLAM Observability Analysis

In the previous section, it was shown that the underlying physical system in SLAM has three unobservable degrees of freedom. Thus, when the EKF is used for state estimation in SLAM, we would expect that the system model employed by the EKF also shares this property. However, in this section we show that this is not the case: the unobservable subspace of the linearized error-state model in the standard EKF is generally of dimension only 2.

Since the linearized error-state model for EKF-SLAM is time-varying, we employ the *local observability matrix* [12] to perform the observability analysis. Specifically, for the EKF-SLAM system considered in this work (cf. (5) and (12)), the local observability matrix for the time interval between time-steps k and $k + m$ is defined as:

$$\mathbf{M} \triangleq \begin{bmatrix} \mathbf{H}_k \\ \mathbf{H}_{k+1}\Phi_k \\ \vdots \\ \mathbf{H}_{k+m}\Phi_{k+m-1}\cdots\Phi_k \end{bmatrix} \quad (20)$$

which can be expanded by substituting the matrices Φ_i and \mathbf{H}_i (cf. (5) and (12), respectively), to yield:

$$\begin{aligned} \mathbf{M} &= \begin{bmatrix} & \mathbf{H}_{R_k} & & \mathbf{H}_{L_k} \\ & \mathbf{H}_{R_{k+1}} \Phi_{R_k} & & \mathbf{H}_{L_{k+1}} \\ & \vdots & & \vdots \\ \mathbf{H}_{R_{k+m}} \Phi_{R_{k+m-1}} \cdots \Phi_{R_k} & & & \mathbf{H}_{L_{k+m}} \end{bmatrix} \quad (21) \\ &= \text{Diag}(\mathbf{H}_{L_k}, \dots, \mathbf{H}_{L_{k+m}}) \times \\ &\quad \underbrace{\begin{bmatrix} & \mathbf{H}_{L_k}^{-1} \mathbf{H}_{R_k} & & \mathbf{I}_2 \\ & \mathbf{H}_{L_{k+1}}^{-1} \mathbf{H}_{R_{k+1}} \Phi_{R_k} & & \mathbf{I}_2 \\ & \vdots & & \vdots \\ \mathbf{H}_{L_{k+m}}^{-1} \mathbf{H}_{R_{k+m}} \Phi_{R_{k+m-1}} \cdots \Phi_{R_k} & & & \mathbf{I}_2 \end{bmatrix}}_{\mathbf{N}} \end{aligned}$$

The system is locally observable over the time period from k to $k+m$ if and only if the local observability matrix \mathbf{M} is full-rank. Since the matrix $\text{Diag}(\mathbf{H}_{L_k}, \dots, \mathbf{H}_{L_{k+m}})$ is nonsingular, it becomes clear that $\text{rank}(\mathbf{M}) = \text{rank}(\mathbf{N})$, and moreover, the matrices \mathbf{M} and \mathbf{N} have the same right nullspace. Therefore, studying the rank and nullspace of \mathbf{N} is equivalent to studying those of \mathbf{M} .

1) *Ideal EKF-SLAM*: Before considering the rank of the matrix \mathbf{M} , which is constructed using the *estimated* values of the state in the filter Jacobians, it is interesting to study the observability properties of the ‘‘oracle’’, or ‘‘ideal’’ EKF (i.e., the filter whose Jacobians are evaluated using the *true* values of the state variables). In the following, all matrices evaluated using the true state values are denoted by the symbol ‘‘ \checkmark ’’.

We start by noting that (cf. (7)):

$$\checkmark\Phi_{R_{k+1}} \checkmark\Phi_{R_k} = \begin{bmatrix} \mathbf{I}_2 & \mathbf{J}(\mathbf{p}_{R_{k+2}} - \mathbf{p}_{R_k}) \\ \mathbf{0}_{1 \times 2} & 1 \end{bmatrix} \quad (23)$$

Based on this property, it is easy to show by induction that:

$$\checkmark\Phi_{R_{k+i-1}} \checkmark\Phi_{R_{k+i-2}} \cdots \checkmark\Phi_{R_k} = \begin{bmatrix} \mathbf{I}_2 & \mathbf{J}(\mathbf{p}_{R_{k+i}} - \mathbf{p}_{R_k}) \\ \mathbf{0}_{1 \times 2} & 1 \end{bmatrix}$$

where $i > 0$. Using this result, and substituting for the measurement Jacobians from (13) and (14), we can prove the following useful identity:

$$\begin{aligned} \checkmark\mathbf{H}_{L_{k+i}}^{-1} \checkmark\mathbf{H}_{R_{k+i}} \checkmark\Phi_{R_{k+i-1}} \cdots \checkmark\Phi_{R_k} \\ = [-\mathbf{I}_2 \quad -\mathbf{J}(\mathbf{p}_L - \mathbf{p}_{R_k})] = \checkmark\mathbf{H}_{L_k}^{-1} \checkmark\mathbf{H}_{R_k} \end{aligned} \quad (24)$$

which holds for all $i > 0$. \mathbf{N} can now be written as

$$\checkmark\mathbf{N} = \begin{bmatrix} \checkmark\mathbf{H}_{L_k}^{-1} \checkmark\mathbf{H}_{R_k} & \mathbf{I}_2 \\ \checkmark\mathbf{H}_{L_k}^{-1} \checkmark\mathbf{H}_{R_k} & \mathbf{I}_2 \\ \vdots & \vdots \\ \checkmark\mathbf{H}_{L_k}^{-1} \checkmark\mathbf{H}_{R_k} & \mathbf{I}_2 \end{bmatrix} = \begin{bmatrix} -\mathbf{I}_2 & -\mathbf{J}(\mathbf{p}_L - \mathbf{p}_{R_k}) & \mathbf{I}_2 \\ -\mathbf{I}_2 & -\mathbf{J}(\mathbf{p}_L - \mathbf{p}_{R_k}) & \mathbf{I}_2 \\ \vdots & \vdots & \vdots \\ -\mathbf{I}_2 & -\mathbf{J}(\mathbf{p}_L - \mathbf{p}_{R_k}) & \mathbf{I}_2 \end{bmatrix}$$

Clearly, $\text{rank}(\checkmark\mathbf{N}) = 2$ and thus the ideal EKF system model is unobservable. Most importantly, however, it can be easily verified that a basis for the right nullspace of $\checkmark\mathbf{N}$ (and thus for the right nullspace of \mathbf{M}) is given by the vectors shown in (18). Thus, the unobservable subspace of the ideal EKF system model is *identical* to the space $d\mathcal{G}^\perp$, that contains the unobservable directions of the nonlinear SLAM system. We

therefore see that if it was possible to evaluate the Jacobians using the true state values, the linearized error-state model employed in the EKF would have observability properties similar to those of the actual, nonlinear SLAM system.

2) *Standard EKF-SLAM*: We now examine the observability properties of the EKF when the Jacobians are evaluated using the latest state estimates, which is the case in a real implementation. We start by deriving an expression analogous to that of (23). We obtain:

$$\Phi_{R_{k+1}} \Phi_{R_k} = \begin{bmatrix} \mathbf{I}_2 & \mathbf{J}(\hat{\mathbf{p}}_{R_{k+2}|k+1} - \hat{\mathbf{p}}_{R_k|k} - \Delta\mathbf{p}_{R_{k+1}}) \\ \mathbf{0}_{1 \times 2} & 1 \end{bmatrix}$$

where $\Delta\mathbf{p}_{R_{k+1}} = \hat{\mathbf{p}}_{R_{k+1}|k+1} - \hat{\mathbf{p}}_{R_{k+1}|k}$ is the correction in the robot position due to the update at time-step $k+1$. Using induction, we can show that:

$$\begin{aligned} \Phi_{R_{k+i-1}} \Phi_{R_{k+i-2}} \cdots \Phi_{R_k} &= \quad (25) \\ \begin{bmatrix} \mathbf{I}_2 & \mathbf{J}(\hat{\mathbf{p}}_{R_{k+i}|k+i-1} - \hat{\mathbf{p}}_{R_k|k} - \sum_{j=k+1}^{k+i-1} \Delta\mathbf{p}_{R_j}) \\ \mathbf{0}_{1 \times 2} & 1 \end{bmatrix} \end{aligned}$$

where $i > 0$. Moreover, we obtain:

$$\begin{aligned} \mathbf{H}_{L_{k+i}}^{-1} \mathbf{H}_{R_{k+i}} \Phi_{R_{k+i-1}} \cdots \Phi_{R_k} \quad (26) \\ = - \begin{bmatrix} \mathbf{I}_2 & \mathbf{J}(\hat{\mathbf{p}}_{L_{k+i}|k+i-1} - \hat{\mathbf{p}}_{R_k|k} + \sum_{j=k+1}^{k+i-1} \Delta\mathbf{p}_{R_j}) \end{bmatrix} \end{aligned}$$

Using this result, we can write matrix \mathbf{N} as:

$$\begin{aligned} \mathbf{N} &= \quad (27) \\ \begin{bmatrix} -\mathbf{I}_2 & -\mathbf{J}(\hat{\mathbf{p}}_{L_{k+1}|k} - \hat{\mathbf{p}}_{R_k|k}) & \mathbf{I}_2 \\ -\mathbf{I}_2 & -\mathbf{J}(\hat{\mathbf{p}}_{L_{k+2}|k+1} - \hat{\mathbf{p}}_{R_k|k} + \Delta\mathbf{p}_{R_{k+1}}) & \mathbf{I}_2 \\ \vdots & \vdots & \vdots \\ -\mathbf{I}_2 & -\mathbf{J}(\hat{\mathbf{p}}_{L_{k+i}|k+i-1} - \hat{\mathbf{p}}_{R_k|k} + \sum_{j=k+1}^{k+i-1} \Delta\mathbf{p}_{R_j}) & \mathbf{I}_2 \end{bmatrix} \end{aligned}$$

At this point, we note that the corrections of the robot position at any given time step are generally nonzero, and additionally, the landmark state estimates at different time instants are not equal. Therefore, the third column of \mathbf{N} will be, in general, a vector with unequal elements, and hence $\text{rank}(\mathbf{N}) = 3$. We thus see that the linearized error-state model employed in the standard EKF-SLAM has different observability properties than the underlying nonlinear system. In particular, by processing the measurements collected in the interval $[k, k+m]$, the EKF acquires information in 3 dimensions of the state space (along the directions corresponding to the observable subspace of the EKF). However, as the nonlinear observability analysis of Section II-B shows, the measurements actually provide information in only 2 directions of the state space. As a result, the EKF gains ‘‘spurious information’’ along the unobservable directions of the underlying nonlinear SLAM system, which leads to inconsistency.

To probe further, we note that the basis of the right nullspace of \mathbf{N} is given by:

$$\text{null}(\mathbf{N}) = [\mathbf{n}_1 \quad \mathbf{n}_2] \quad (28)$$

which, as explained in Section II-B corresponds to a shifting of the $x-y$ plane. It is interesting to point out that the ‘‘missing’’

direction in the unobservable subspace of the EKF system model is the one along the vector \mathbf{n}_3 , which corresponds to a rotation of the $x-y$ plane. Therefore, we see that the filter will gain “nonexistent” information about the robot’s orientation. This will lead to an unjustified reduction in the uncertainty of the robot’s orientation, which will, in turn, further reduce the uncertainty in all the state variables. This agrees in some respects with [2], [5], where it was argued that the orientation uncertainty is the major cause of the filter’s inconsistency. However, we point out that the *root cause* of the problem is the fact that the Jacobians are evaluated at different linearization points at every time step. This changes the dimension of the observable subspace, and thus fundamentally alters the properties of the estimation process.

An additional interesting point is that the covariance matrix of the measurements does not appear in the observability analysis of the filter. Therefore, even if this covariance matrix is artificially inflated, the filter will retain the same observability properties (i.e., the same observable and unobservable subspaces). This shows that no amount of covariance inflation can result in correct observability properties. Similarly, even if the Iterated EKF is employed for state estimation, the same, erroneous, observability properties will arise, since the landmark position estimates will generally differ at different time steps.

As a final remark, we note the “correct” observability properties of the ideal EKF are attributed to the fact that (24) holds, which is not the case for the standard EKF. When condition (24) is met, it ensures that all the block rows of the matrix \mathbf{N} are identical, and leads to an unobservable subspace of dimension three. Thus, (24) can be seen as a sufficient condition that, when satisfied by the filter Jacobians, ensures correct observability properties. Interestingly, as shown in [11], (24) is equivalent to the condition derived in [3] (cf. Theorem 1 therein), for the case where the robot remains stationary. This indicates that the Jacobian constraint (24) derived based on the observability criterion is more general, and encompasses the constraint of [3] as a special case.

III. FIRST-ESTIMATES JACOBIAN EKF SLAM

Careful observation of the matrix \mathbf{N} in (27) reveals that it is possible to obtain an EKF system model with an unobservable subspace of dimension three, even if the Jacobians are not evaluated at the true state values. For this purpose, the following two changes are necessary.

- 1) Instead of computing the state-propagation Jacobian matrix Φ_{R_k} as in (7), we employ the expression:

$$\Phi'_{R_k} = \begin{bmatrix} \mathbf{I}_2 & \mathbf{J}(\hat{\mathbf{p}}_{R_{k+1|k}} - \hat{\mathbf{p}}_{R_{k|k-1}}) \\ \mathbf{0}_{1 \times 2} & 1 \end{bmatrix} \quad (29)$$

The difference compared to (7) is that the robot position estimate prior to updating, $\hat{\mathbf{p}}_{R_{k|k-1}}$, is employed in this computation instead of the updated estimate, $\hat{\mathbf{p}}_{R_{k|k}}$.

- 2) In the evaluation of the measurement Jacobian matrix \mathbf{H}_{R_k} (cf. (13)) we always utilize the landmark estimate *from the first time* the landmark was detected. Thus, if a landmark was first seen at time-step ℓ , we compute the

measurement Jacobian with respect to the robot pose as:

$$\mathbf{H}'_{R_k} = (\nabla \mathbf{h}_k) \mathbf{C}^T (\hat{\phi}_{R_{k|k-1}}) \begin{bmatrix} -\mathbf{I}_2 & -\mathbf{J}(\hat{\mathbf{p}}_{L_{\ell|k}} - \hat{\mathbf{p}}_{R_{k|k-1}}) \end{bmatrix} \quad (30)$$

As a result of the above modifications, only the *first* estimates of all landmark positions and all robot poses appear in the Jacobians of the filter. This has as effect that the observability matrix \mathbf{N} of this new filter, which we term *First-Estimates Jacobian* (FEJ)-EKF, assumes the form:

$$\mathbf{N}' = \begin{bmatrix} -\mathbf{I}_2 & -\mathbf{J}(\hat{\mathbf{p}}_{L_{\ell|k}} - \hat{\mathbf{p}}_{R_{k|k-1}}) & \mathbf{I}_2 \\ -\mathbf{I}_2 & -\mathbf{J}(\hat{\mathbf{p}}_{L_{\ell|k}} - \hat{\mathbf{p}}_{R_{k|k-1}}) & \mathbf{I}_2 \\ -\mathbf{I}_2 & -\mathbf{J}(\hat{\mathbf{p}}_{L_{\ell|k}} - \hat{\mathbf{p}}_{R_{k|k-1}}) & \mathbf{I}_2 \\ \vdots & \vdots & \vdots \\ -\mathbf{I}_2 & -\mathbf{J}(\hat{\mathbf{p}}_{L_{\ell|k}} - \hat{\mathbf{p}}_{R_{k|k-1}}) & \mathbf{I}_2 \end{bmatrix}$$

This matrix is of rank 2, and thus the FEJ-EKF is based on an error-state system model whose unobservable subspace is of dimension 3. We stress that the FEJ-EKF estimator is realizable “in the real world”, since it does not utilize any knowledge of the true state. Interestingly, even though this new filter does not use the latest available state estimates (and thus utilizes Jacobians that are less accurate than those of the standard EKF), it exhibits better consistency properties than the standard EKF, as shown in the following section.

IV. SIMULATION RESULTS

A series of Monte-Carlo comparison studies were conducted under various conditions, in order to validate the preceding theoretical analysis and to demonstrate the capability of the FEJ-EKF filter to improve the consistency of EKF-SLAM. The metrics used to evaluate filter performance are: (i) the RMS error, and (ii) the average normalized (state) estimation error squared (NEES) [6]. Specifically, for the landmarks we compute the average RMS and average NEES errors by averaging the squared errors and the NEES, respectively, over all Monte Carlo runs, all landmarks and all time steps. On the other hand, for the robot pose we compute these error metrics by averaging over all Monte Carlo runs for each time step (cf. [11] for a more detailed description).

The RMS of estimation errors provide us with a concise metric of the accuracy of a given estimator. On the other hand, the NEES is a powerful metric for evaluating filter consistency. Specifically, it is known that the NEES of an M -dimensional Gaussian random variable follows a χ^2 distribution with M degrees of freedom. Therefore, if a certain filter is consistent, we expect that the average NEES for the robot pose will be close to 3 for all k , and that the average landmark NEES will be close to 2. The larger the deviations of the NEES from these values, the larger the inconsistency of the filter. By studying both the RMS errors and NEES of all the filters, we obtain a comprehensive picture of the estimators’ performance.

In all the simulation tests presented in this section, the robot moves at a constant velocity of $v = 0.25$ m/sec, the standard deviation of the velocity measurement noise is equal to $\sigma_v = 0.1v$, while the rotational velocity measurements are corrupted by noise with standard deviation $\sigma_\omega = 1^\circ/\text{sec}$. The robot records measurements of the relative position of

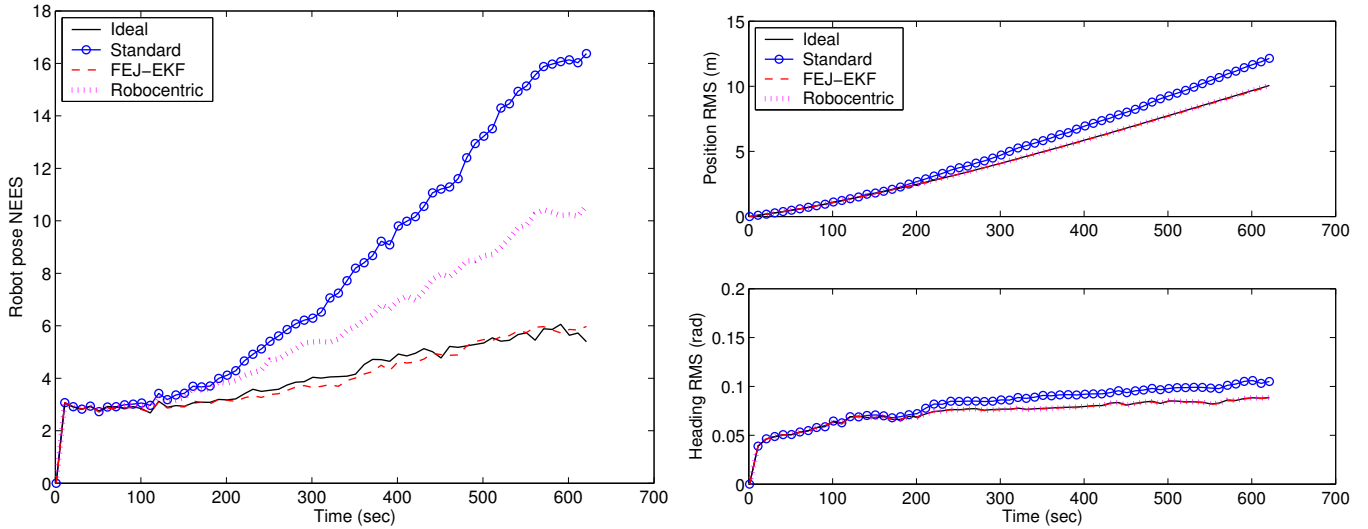


Fig. 1. Monte Carlo results for an exploration-SLAM scenario. (a) Average NEES of the robot pose errors (b) RMS errors for the robot pose (position and orientation). In these plots, the solid lines correspond to the ideal EKF, the dashed lines to the FEJ-EKF, the solid lines with circles to the standard EKF, and the dotted lines to the robocentric mapping algorithm of [4]. Note that the RMS errors of the ideal EKF, the FEJ-EKF, and the robo-centric SLAM algorithm are almost identical, which makes the corresponding lines difficult to distinguish.

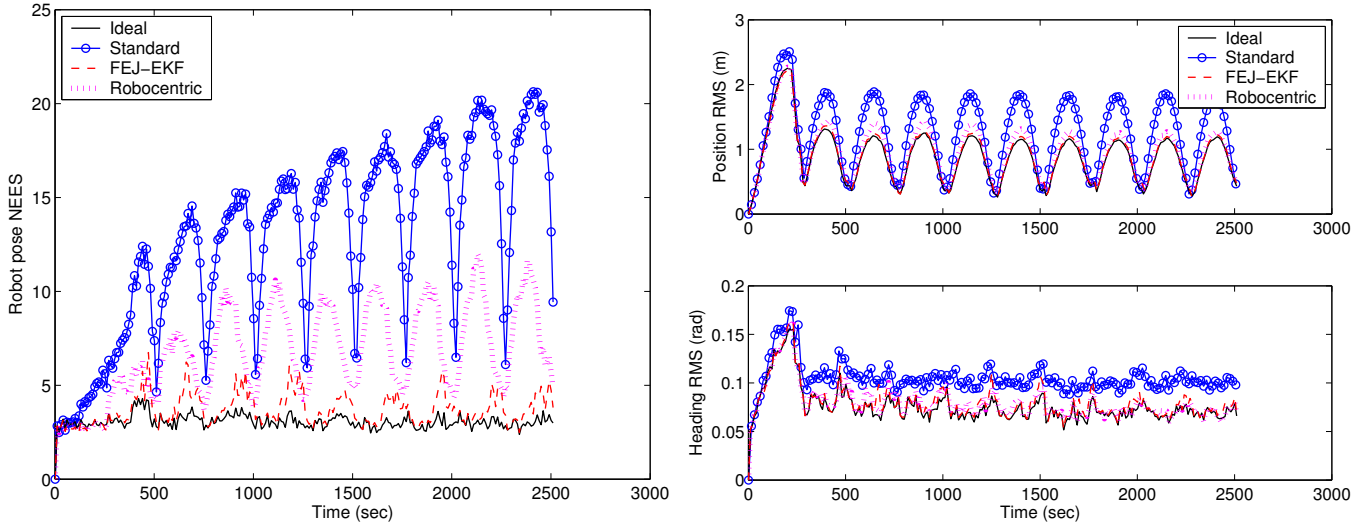


Fig. 2. Monte Carlo results for a SLAM scenario with multiple loop closures. (a) Average NEES of the robot pose errors (b) RMS errors for the robot pose (position and orientation). In these plots, the solid lines correspond to the ideal EKF, the dashed lines to the FEJ-EKF, the solid lines with circles to the standard EKF, and the dotted lines to the robocentric mapping algorithm of [4]. Note that the RMS errors of the ideal EKF and the FEJ-EKF are almost identical, which makes the corresponding lines difficult to distinguish.

landmarks that lie within its sensing range of 5 m, with standard deviation equal to 15% of the robot-to-landmark distance along each axis. 100 Monte Carlo simulations were performed, and during each run, four filters process the same data, to ensure a fair comparison. The four filters compared are: (i) the ideal EKF, (ii) the standard EKF, (iii) the FEJ-EKF, and (iv) the robocentric filter [1], [4], which aims at improving the consistency of SLAM by expressing the landmarks in a robot-relative frame. It should be pointed out that the sensor-noise levels selected for the simulations are larger than what is typically encountered in practice. This was done since larger noise levels lead to higher estimation errors, which in turn cause the Jacobian estimates to be less accurate, and

make the effects of inconsistency more apparent. Two SLAM scenarios are considered: exploration SLAM and SLAM with loop closure. In the first case, the robot constantly explores unseen territory, without returning to already revisited areas. At the end of each run, approximately 40 landmarks have been detected. In the second case, the robot executes 10 loops on a circular trajectory, and observes 20 landmarks in total. The comparative results for all filters are presented in Figs. 1 and 2, and Tables I and II. Specifically, Fig. 1(a) and Fig. 1(b) show the average NEES and RMS errors for the robot pose, respectively, for the case of exploration SLAM. Fig. 2(a) and Fig. 2(b) show the same quantities for the circular trajectory. On the other hand, Tables I and II present the average values of

	Ideal EKF	Std. EKF	FEJ-EKF	[4]
Position Err. RMS (m)				
Explor.	22.41	32.73	22.65	22.73
Loops	0.95	2.08	0.98	1.16
NEES				
Explor.	2.58	6.70	2.66	4.32
Loops	2.1	12.93	2.35	6.65

TABLE I
LANDMARK POSITION ESTIMATION PERFORMANCE

	Ideal EKF	Std. EKF	FEJ-EKF	[4]
Position Err. RMS (m)				
Explor.	3.86	4.61	3.87	3.89
Loops	0.69	0.98	0.70	0.75
Heading Err. RMS (rad)				
Explor.	0.074	0.084	0.074	0.074
Loops	0.079	0.11	0.082	0.082
NEES				
Explor.	4.16	8.05	4.07	5.92
Loops	3.05	12.79	3.68	6.70

TABLE II
ROBOT POSE ESTIMATION PERFORMANCE

all relevant performance metrics for the landmarks and robot respectively, for both simulation scenarios. Several interesting conclusions can be drawn from these results. First, it becomes clear that the performance of the FEJ-EKF is *almost identical* to that of the ideal EKF, and substantially better than the standard EKF, both in terms of RMS errors and NEES. This occurs even though the Jacobians used in the FEJ-EKF are less accurate than those used in the standard EKF, as explained in the preceding section. This fact indicates that the errors introduced by the use of inaccurate Jacobians have a less detrimental effect on consistency than the use of an error-state system model with observable subspace of dimension larger than that of the actual, nonlinear, SLAM system.

A second observation is that the FEJ-EKF also performs better than robocentric mapping [4], both in terms of accuracy and in terms of consistency. One possible justification for this is based on the fact that in robocentric mapping, during each propagation step *all* landmark position estimates need to be changed, since they are expressed with respect to the moving robot frame. As a result, during each propagation step (termed *composition* in [4]), all landmark estimates and their covariance are affected by the linearization errors of the process model. This problem does not exist in the world-centric formulation of SLAM, and it could offer an explanation for the observed behavior. As a final remark, we note that even though the FEJ-EKF NEES performance is significantly better compared to that of the robocentric mapping, the difference in the RMS errors of the two filters is less pronounced. This indicates that the effects of inconsistency primarily affect the covariance, rather than the state estimates.

V. CONCLUSIONS

In this paper, we have studied in depth the issue of filter inconsistency in EKF-based SLAM, from an observability perspective. By comparing the observability properties of the nonlinear SLAM system model with those of the linearized error-state model employed in the EKF, we proved that the observable subspace of the standard EKF is always of higher dimension than the observable subspace of the underlying nonlinear system. As a result, the covariance estimates of the EKF undergo reduction in directions of the state space where no information is available, which is a primary cause of inconsistency. Based on the above analysis, a new “First Estimates Jacobian” (FEJ) EKF is proposed to improve the estimator’s consistency during SLAM. The proposed algorithm performs better with respect to consistency, because when the filter Jacobians are calculated using the first available estimate for each state variable, the error-state system model has an observable subspace of the same dimension as the underlying nonlinear SLAM system. Through extensive Monte-Carlo simulations we have verified that the FEJ-EKF is more accurate and more consistent than both the standard EKF and robocentric mapping [4], which has been proposed for improving estimator consistency in SLAM.

ACKNOWLEDGMENT

This work was supported by the University of Minnesota (DTC) and the National Science Foundation (EIA-0324864, IIS-0643680).

REFERENCES

- [1] J. Castellanos, R. Martinez-Cantin, J. Tardos, and J. Neira, “Robocentric map joining: Improving the consistency of EKF-SLAM,” *Robotics and Autonomous Systems*, vol. 55, pp. 21–29, 2007.
- [2] T. Bailey, J. Nieto, J. Guivant, M. Stevens, and E. Nebot, “Consistency of the EKF-SLAM algorithm,” in *IEEE/RSJ International Conference on Intelligent Robots and Systems (IROS)*, Beijing, China, October 2006, pp. 3562–3568.
- [3] S. Julier and J. Uhlmann, “A counter example to the theory of simultaneous localization and map building,” in *IEEE International Conference on Robotics and Automation (ICRA)*, 2001, pp. 4238–4243.
- [4] J. Castellanos, J. Neira, and J. Tardos, “Limits to the consistency of EKF-based SLAM,” in *5th IFAC Symposium on Intelligent Autonomous Vehicles*, Lisbon, Portugal, July 2004.
- [5] S. Huang and G. Dissanayake, “Convergence analysis for extended Kalman filter based SLAM,” in *IEEE Conference on Robotics and Automation (ICRA)*, Orlando, Florida, May 2006, pp. 412–417.
- [6] Y. Bar-Shalom, X. R. Li, and T. Kirubarajan, *Estimation with applications to tracking and navigation*. New York: Wiley, 2001.
- [7] J. Andrade-Cetto and A. Sanfeliu, “The effects of partial observability in SLAM,” in *IEEE International Conference on Robotics and Automation (ICRA)*, New Orleans, LA, April 2004, pp. 394–402.
- [8] —, “The effects of partial observability when building fully correlated maps,” *IEEE Transactions on Robotics*, vol. 21, no. 4, pp. 771–777, 2005.
- [9] K. W. Lee, W. S. Wijesoma, and J. I. Guzman, “On the observability and observability analysis of SLAM,” in *IEEE/RSJ International Conference on Intelligent Robots and Systems (IROS)*, Beijing, China, October 2006, pp. 3569–3574.
- [10] R. Hermann and A. Krener, “Nonlinear controllability and observability,” *IEEE Transactions on Automatic Control*, vol. 22, pp. 728–740, 1977.
- [11] G. Huang, A. Mourikis, and S. Roumeliotis, “Analysis and improvement of the consistency of extended Kalman filter based SLAM,” University of Minnesota, Minneapolis, MN, Tech. Rep., August 2007, www.cs.umn.edu/~mourikis/tech_reports/TR_consistency.pdf.
- [12] Z. Chen, K. Jiang, and J. C. Hung, “Local observability matrix and its application to observability analyses,” in *16th Annual Conference of IEEE (IECON’90)*, Pacific Grove, CA, USA, November 1990, pp. 100–103.